Quantum Mechanical Dynamical Effects in an Enzyme-Catalyzed Proton Transfer Reaction

Cristóbal Alhambra,[†] Jiali Gao,[†] José C. Corchado,[‡,||] Jordi Villà,[‡,§] and Donald G. Truhlar*,[⊥]

Contribution from the Department of Chemistry, State University of New York at Buffalo, Buffalo, New York 14260, Departamento de Química Física, Universidad de Extremadura, 06071 Badajoz, Spain, Departament de Química, Universitat Autònoma de Barcelona, 08193 Bellaterra (Barcelona), Spain, and Department of Chemistry and Supercomputer Institute, University of Minnesota, Minneapolis, Minnesota 55455

Abstract: We have calculated the reaction rate and kinetic isotope effects for conversion of 2-phospho-D-glycerate to phosphoenolpyruvate by yeast enolase. The potential energy surface is modeled by a combined quantum mechanical/molecular mechanical method with generalized hybrid orbitals. The dynamics calculations are carried out by semiclassical variational transition state theory with multidimensional tunneling contributions. Quantum effects are included for a 25-atom cluster consisting of the substrate and part of the protein embedded in a rigid framework consisting of the rest of the protein and water. Quantum effects are important for calculating the absolute rate constant, and variational optimization of the dynamical bottleneck location is important for calculating the kinetic isotope effects. This provides the first evidence that transition state geometries are isotope dependent for enzyme reactions.

1. Introduction

A large number of enzyme-catalyzed reactions proceed by proton transfer or hydride transfer,[1] but the widely employed classical-trajectory molecular dynamics simulation methods[2,3] neglect the effects of quantum mechanical zero-point energy and tunneling which are expected to be important when hydrogenic coordinates participate in the reaction coordinate. Semiclassical variational transition state theory[4−6] (SC-VTST), which is VTST with quantized vibrational partition functions and semiclassical multidimensional tunneling contributions, includes these effects but has so far not been applied to enzyme reactions. The present paper reports such an application for a key enzyme reaction in glucose fermentation, namely the conversion of 2-phospo-D-glycerate (2-PGA) to phosphoenolpyruvate (PEP),[1] which proceeds by proton transfer, and for the kinetic isotope effect (KIE) for deuteron transfer.

Enolase is a glycolytic enzyme that catalyzes the reversible dehydration of 2-PGA to PEP. Primary and secondary KIEs have given strong evidence for a stepwise carbanionic mechanism involving the initial formation of a carbanion intermediate by abstraction of the weak acid proton on the α carbon (C-2).[7,8] Activity assays with the wild type and several mutants[9] have identified the ϵ-nitrogen on the enzyme residue Lys 345 as the general base catalyst for proton abstraction. A detailed picture of the overall process catalyzed by enolase has emerged from its high-resolution X-ray structure.[10,11] The X-ray structure provides insights into the function of active site residues and is consistent with the hypothesis of a stepwise mechanism, as shown in Scheme 1, where E-B denotes the enzyme base. The proton-transfer step (first reaction step in Scheme 1) has a high kinetic barrier and is the primary rate-limiting step.[8] The rest of this paper is concerned with this elementary step. The high

† State University of New York at Buffalo.
‡ Department of Chemistry, University of Minnesota.
|| Universidad de Extremadura.
§ Universitat Autònoma de Barcelona.
⊥ Department of Chemistry and Supercomputer Institute, University of Minnesota.
(1) Walsh, C. *Enzymatic Reaction Mechanisms*; Freeman: San Francisco, 1979.
(2) Brooks, B. R.; Bruccoleri, R. E.; Olafson, B. D.; States, D. J.; Swaminathan, S.; Karplus, M. J. *J. Comput. Chem.* **1983**, *4*, 187−217.
(3) (a) McCammon, J. A.; Harvey, S. C. *Dynamics of Proteins and Nucleic Acids*; Cambridge University Press: New York, 1987. (b) Van Gunsteren, W. F.; Berendsen, H. J. C. *Angew. Chem., Int. Ed. Engl.* **1990**, *29*, 992. (c) Parrinello, M. In *Modern Techniques in Computational Chemistry: MOTECC-91*; Clementi, E., Ed.; ESCOM: Leiden, 1991; pp 833−845. (d) Corongiu, G.; Aida, M.; Pas, M. F.; Clementi, E. In *Modern Techniques in Computational Chemistry: MOTECC-91*; Clementi, E., Ed.; ESCOM: Leiden, 1991; pp 847−919. (e) Pearlman, D. A.; Case, D. A.; Caldwell, J. W.; Ross, W. S.; Cheatham, T. E., III; DeBolt, S.; Ferguson, D.; Seibel, G.; Kollman, P. *Computer Phys. Commun.* **1995**, *91*, 1−41. (f) Bolton, K.; Hase, W. L.; Peslherbe, G. H. In *Modern Methods for Multidimensional Dynamics Computations in Chemistry*; Thompson, D. L., Ed.; World Scientific: Singapore, 1998; pp 143−189. (g) Stanton, R. V.; Miller, J. L.; Kollman, P. A. In *Modern Methods for Multidimensional Dynamics Computations in Chemistry*; Thompson, D. L., Ed.; World Scientific: Singapore, 1998; pp 355−383.
(4) Truhlar, D. G.; Garrett, B. C. *Acc. Chem. Res.* **1980**, *13*, 440−448.
(5) Truhlar, D. G.; Isaacson, A. D.; Skodje, R. T.; Garrett, B. C. *J. Phys. Chem.* **1982**, *86*, 2252−2261.
(6) (a) Truhlar, D. G.; Garrett, B. C. *Annu. Rev. Phys. Chem.* **1984**, *35*, 159−189. (b) Tucker, S. C.; Truhlar, D. G. *NATO ASI SER. C* **1989**, *267*, 291−346. (c) Allison, T. C.; Truhlar, D. G. In *Modern Methods for Multidimensional Dynamics Computations in Chemistry*; World Scientific: Singapore, 1998; pp 618−712.
(7) Dinovo, E. C.; Boyer, P. D. *J. Biol. Chem.* **1971**, *246*, 4586−4593.
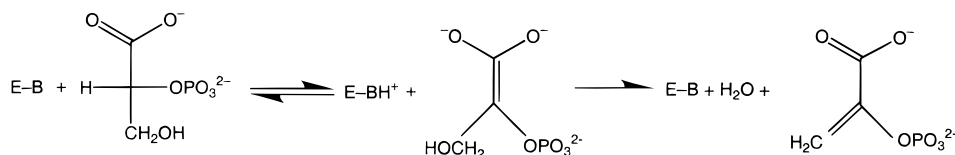(8) Anderson, S. R.; Anderson, V. E.; Knowles, J. R. *Biochemistry* **1994**, *33*, 10545−10555.
(9) Poyner, R. R.; Laughlin, L. T.; Sowa, G. A.; Reed, G. H. *Biochemistry* **1996**, *35*, 1692−1699.
(10) Larsen, T. M.; Wedeking, J. E.; Rayment, I.; Reed, G. H. *Biochemistry* **1996**, *35*, 4349−4358.
(11) Weedekind, J. E.; Reed, G. H.; Rayment, I. *Biochemistry* **1995**, *34*, 4325−4330.
(12) Gerlt, J. A.; Gassman, P. G. *J. Am. Chem. Soc.* **1992**, *114*, 5928−5934.

Scheme 1

barrier is not surprising in light of the low acidity of the C-2 proton of carboxylate anions ($pK_a \gtrsim 32$).[12]

The catalytic reaction of wild-type yeast enolase has been characterized as follows: The equilibrium constant is near unity,[13] corresponding to $\Delta G \approx 0$. The rate constant is[9] 78 s^{-1}, corresponding to $\Delta G_T^{act} \approx 15$ kcal/mol, where the phenomenological definition[14] of the free energy of the activation ΔG_T^{act} for a unimolecular reaction is

$$k(T) = \frac{\tilde{k}T}{h} \exp(-\Delta G_T^{act}/RT) \qquad (1)$$

where $k(T)$ is the rate constant at temperature T, $\tilde{k}$ is Boltzmann's constant, h is Planck's constant, and R is the gas constant. The KIE for deuteron transfer is[8] $k_H/k_D = 3.3$.

2. Potential Energy Function

The potential energy surface was calculated by a mixed quantum mechanical/molecular mechanical (QM/MM) method.[15,16] The system (N atoms) was partitioned into N_{QM} quantum mechanical atoms and N_{MM} classical mechanical atoms. The quantum mechanical atoms consisted of the 15-atom substrate and the $H_2N-C_\epsilon H_2-C_\delta H_2-C_\gamma$ portion of the Lys 345 side chain. Thus $N_{QM} = 25$. The remainder of the system consists of 6934 more protein atoms plus crystallographic and some (see below) bulk water (643 water molecules in all), for a total of 8863 classical atoms. The QM subsystem was described by the AM1 model.[17] The rest of the protein atoms and the two magnesium ions in the active site (which coordinate the carboxylate and the phosphate of the 2-PGA) were represented by using the CHARMM22 MM force field,[18] and the water was modeled by the TIP3P[19] MM force field.

The boundary between the QM and MM partition, which is located on the C$_\gamma$ atom of Lys 345, was modeled with a recently developed[16] generalized hybrid orbital (GHO) method. The GHO method avoids the use of hydrogenic link atoms or capping atoms, and it provides a well-defined potential energy surface that can be used for energy minimization and molecular dynamics simulations. Unlike the link-atom approach, the GHO method avoids adding extra degrees of freedom to the system.

The performance of the AM1 model for the quantum mechanical subsystem of the present kind of reaction was

(13) Burbaum, J. J.; Knowles, J. R. *Biochemistry* **1989**, *28*, 9306−9317.
(14) (a) Hammes, G. G. *Principles of Chemical Kinetics*; Academic: New York, 1978; p 56. (b) Kreevoy, M. M.; Truhlar, D. G. *Techniques Chem. (N.Y.)*; 4th ed., **1986**, *6*/Part 1, 13−95. (c) Truhlar, D. G.; Garrett, B. C. *J. Am. Chem. Soc.* **1989**, *111*, 1232−1236.
(15) Bash, P. A.; Field, M. J.; Karplus, M. *J. Am. Chem. Soc.* **1987**, *109*, 8092−8094.
(16) Gao, J.; Amara, P.; Alhambra, C.; Field, M. J. *J. Phys. Chem. A* **1998**, *102*, 4714−4721.
(17) Dewar, M. J. S.; Zoebisch, E. G.; Healy, E. F.; Stewart, J. J. P. *J. Am. Chem. Soc.* **1985**, *107*, 3902−3909.
(18) MacKerell, A. D., Jr.; Bashford, D.; Bellott, M.; Dunbrack, R. L., Jr.; Evanseck, J. D.; Field, M. J.; Gao, J.; Guo, H.; Ha, S.; Joseph-McCarthy, D.; Kuchnir, L.; Kuczera, K.; Lau, F. T. K.; Mattos, C.; Michnick, S.; Ngo, T.; Nguyen, D. T.; Prodhom, B.; Reiher, W. E., III; Roux, B.; Schlenkrich, M.; Smith, J. C.; Stote, R.; Straub, J.; Watanabe, M.; Wiórkievicz-Kuczera, J.; Yin, D.; Karplus, M. *J. Phys. Chem. B* **1998**, *102*, 3586−3616.
(19) Jorgensen, W. L.; Chandrasekhar, J.; Madura, J. D.; Impey, R. W.; Klein, M. L. *J. Chem. Phys.* **1983**, *79*, 926−935.

investigated by comparison to calculations by the Hartree−Fock molecular orbital method[20] with the 6-31+G* basis set for the gas-phase process $CH_3NH_2 + CH_3CH_2COO^- \rightarrow CH_3NH_3^+ + CH_3CHCOO^{2-}$. The zero-point-exclusive endoergicity is calculated to be 293 kcal/mol at the HF/6-31+G* level and 288 kcal/mol at the AM1 level. This model reaction has the deficiency that the dianion is not stable in the gas phase; nevertheless, the comparison suggests that the semiempirical AM1 model is not too unreasonable compared to higher-level calculations for this kind of process.

There are two Mg^{2+} atoms in the protein, one strongly bound to the protein and substrate, and the other loosely bound. The strongly bound Mg^{2+} is coordinated by Glu 295, Asp 246, and Asp 320, bidentate interaction with the two carboxylate oxygens of 2-PGA, and a water molecule. The loosely bound Mg^{2+} is simultaneously coordinated to one of the carboxylate oxygens of the substrate from the anti position and one oxygen of the phosphate group; three other coordination sites are filled by two water molecules and the side chain oxygen of Ser 39, as in the X-ray structure of the crystal of the enzyme bound to an equilibrium mixture of 2-PGA and PEP.[10] The sixth coordination site of the second Mg^{2+} is occupied by the ester oxygen of the phosphate, as compared to the crystal, where it is filled by the backbone (carbonyl) oxygen of Ser 39.

3. Dynamics

The dynamics calculation proceeds in two stages; the first step is classical mechanical (CM), and the second step is semiclassical (SC). The key element in the second step is a partition of the N-atom total system into N_1 primary-zone atoms and N_2 secondary-zone atoms, where $N_1 + N_2 = N$. In the CM step, all N atoms have thermal energy. In the SC step the N_1 primary-zone atoms are treated as a cluster embedded in a rigid framework,[21] and only the cluster atoms have kinetic energy. The effect of the rigid framework on the active atoms in the SC step is simply to provide a static potential field. For the present application the cluster was taken to be identical to the QM subsystem (so $N_1 = N_{QM}$ and $N_2 = N_{MM}$), but this is not required in general.

The system was initialized with the crystal structure (at 1.8 Å resolution) for the yeast enolase complexed with an equilibrium mixture of 2-PGA/PEP structures[10] (this is structure 1ONE in the Brookhaven Protein Database). Hydrogen positions for the protein residues and crystallographic waters were built with the HBUILD module in CHARMM.[2] The final structure was subjected to 500 cycles of Newton−Raphson energy minimization to relax any possible bad contacts in the initial crystal positions. Then a 24 Å sphere of equilibrated waters was centered at the C-2 position. Note that this sphere is not large enough to encompass the entire protein in all directions. Water molecules at a distance smaller than 2.6 Å from any protein atom or crystallographic water were removed.

Then a CM molecular dynamics simulation was carried out at 300 K with a locally modified version of the CHARMM

(20) Hehre, W. J.; Radom, L.; Schleyer, P. v. R.; Pople, J. A. *Ab Initio Molecular Orbital Theory*; Wiley: New York, 1986.
(21) Lauderdale, J. G.; Truhlar, D. G. *J. Chem. Phys.* **1986**, *84*, 1843−1849.

program.[2] The CM calculations were carried out by stochastic boundary molecular dynamics.[22−24] After 50 ps of equilibration, an additional 10 ps simulation was executed with strong harmonic constraints on the breaking C−H bond distance r_1 at a value of 1.58 Å and on the forming N−H bond distance r_2 at a value of 1.21 Å. The purpose of this CM step is simply to generate a typical configuration for starting the SC step. The criterion used was that the bath structure chosen should lead to a barrier height and energy of reaction that provides a qualitatively reasonable representation of the experimental situation. For the configuration we chose, we froze the secondary-zone atoms and optimized the primary-zone atoms for the three stationary points, i.e., reactants, saddle point, and products. The optimizations were carried out by the BFGS method[25] for reactants and products and by the Newton−Raphson method with Brent line minimization[26] for the saddle point. The structure of the reactant molecule in the active site is illustrated in Figure 1A, along with the two Mg^{2+} ions, and the active part of the catalytic lysine, and Figure 2B shows the product of the elementary step under study here. We found that the barrier height for the reaction of the embedded cluster is 17.0 kcal/mol, and the reaction is 2.6 kcal/mol endoergic. Using the harmonic approximation and adding zero-point energy for the primary-zone atoms changes these values to $\Delta H_0^{\ddagger} = 14.4$ kcal/mol and $\Delta H_0 = 2.6$ kcal, respectively. Finally, using the harmonic approximation for calculating quantal partition functions and adding thermal contributions for the primary-zone atoms yields $\Delta G_{300}^{\ddagger} = 14.5$ kcal/mol and $\Delta G_{300} = 2.8$ kcal/mol. Note that these values for $\Delta H_0^{\ddagger}$ and $\Delta G_{300}^{\ddagger}$ are calculated using the saddle point structure and hence correspond to conventional transition state theory. The values for $\Delta G_0^{\ddagger}$ and

(22) Brooks, C. L.; Brünger, A.; Karplus M. *Biopolymers* **1985**, *24*, 843−865. There are three concentric regions centered at the C-2 position of the substrate: a 20 Å sphere called the reactant region, which is treated by Hamiltonian dynamics, a spherical shell from 20 to 24 Å called the buffer on heat-bath region, in which forces due to explicit interactions with other particles are augmented by stochastic Langevin forces (friction and a random force), and an outer region called the reservoir boundary region. In addition, protein atoms in the buffer and reservoir regions are constrained by a harmonic restoring force based on a reference position; the force constant is 1.0 kcal mol^{-1} Å^{-2}. Water molecules are not harmonically constrained. The reaction region plus the buffer region constitute the simulation zone. The assignment of atoms in the simulation zone to one of these regions is updated every 5 time steps. Initially the reaction region has 4068 atoms, of which 852 are in 284 water molecules. Initially the buffer region has 3050 atoms, of which 1077 are in 359 water molecules. The reservoir has 1230 atoms. The SHAKE algorithm[23] was used to constrain all bonds involving hydrogens in the MM subsystem. The integration time step was 1 fs, and a cutoff of 14 Å was used to evaluate nonbonded interactions based on a group switched scheme.[24]
(23) Ryckaert, J.-P.; Cicotti, G.; Berendsen, H. J. C. *J. Comput. Phys.* **1977**, *23*, 327−341.
(24) Brooks, C. L., III; Pettit, B. M.; Karplus, M. *J. Chem. Phys.* **1985**, *83*, 5897−5908.
(25) Broyden, C. G. *J. Inst. Math. Appl.* **1970**, *6*, 76. Fletcher, R. *Comput. J.* **1970**, *13*, 317. Goldfarb *Math Comp.* **1970**, *24*, 23. Shanno, D. F. *Math. Comp.* **1970**, *24*, 647.
(26) Press, W. H.; Flannery, S. P.; Teukolsky, S. A.; Vetterling, W. T. *Numerical Recipes*; Cambridge University Press: Cambridge, 1986; p 254.
(27) Corchado, J. C.; Alhambra, C.; Villà, J.; Gao, J.; Truhlar, D. G. CHARMMRATE-version 0.1; State University of New York at Buffalo and University of Minnesota, Minneapolis, 1998. A distribution version (1.0) of the CHARMMRATE interface of POLYRATE to CHARMM is in preparation, and it will be distributed as a module of CHARMM when it is available.
(28) (a) Steckler, R.; Hu, W.-P.; Liu, Y.-P.; Lynch, G. C.; Garrett, B. C.; Isaacson, A. D.; Melissas, V. S.; Lu, D.-h.; Truong, T. N.; Rai, S. N.; Hancock, G. C.; Lauderdale, J. G.; Joseph, T.; Truhlar, D. G. *Comput. Phys. Commun.* **1995**, *88*, 341−343. (b) Corchado, J. C.; Chuang, Y.-Y.; Fast, P. L.; Villà, J.; Coitiño, E. L.; Hu, W.-P.; Liu, Y.-P.; Lynch, G. C.; Nguyen, K. A.; Jackels, C. F.; Gu, M. Z.; Rossi, I.; Clayton, S.; Melissas, V. S.; Steckler, R.; Garrett, B. C.; Isaacson, A. D.; Truhlar, D. G. POLYRATE-version 7.9.1, University of Minnesota, Minneapolis, 1998.
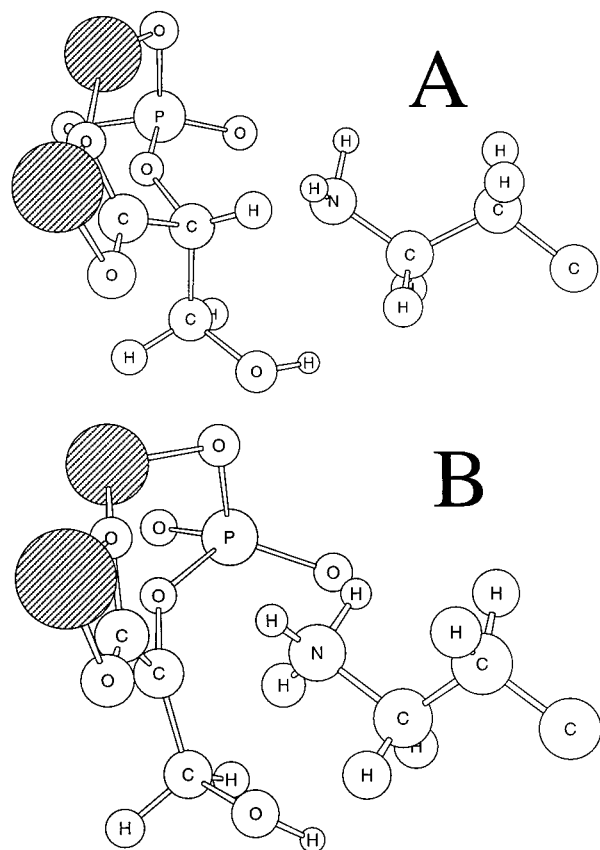
Figure 1. (A) The optimized structure of the reactant of the elementary reaction under study here. The reactant was optimzed in the field of the enzyme and included water molecules. The figure shows the substrate plus part of the enzyme, in particular the two Mg^{2+} atoms and the part of the lysine residue that is treated as active in the semiclassical step. (B) Same as A except the product.
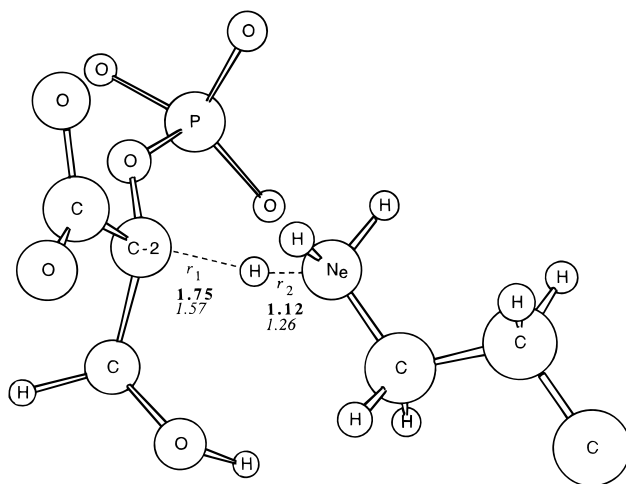
Figure 2. The optimal structure of the quantum mechanical subsystem at the CVT transition state for proton transfer. The values of r_1 and r_2 for the proton transfer (bold) and deuteron transfer (italic) are given in Å.

ΔG_{300} obtained in this way are in reasonably good agreement with the experimental values mentioned in Section 1, and this indicates that this structure for the protein−water framework (unlike others we examined) is reasonably representative of wild-type yeast enolase. Hence we accepted this structure for use in the SC step described next.

The SC step was carried out using CHARMMRATE,[27] which is an interface of CHARMM[2] and POLYRATE.[28] During the

SC step, the secondary-zone atoms were frozen at the structure described above. The reaction path[5] for primary-zone atoms was calculated by the Euler[29] steepest descent method in mass-scaled coordinates. Vibrational partition functions and generalized free energies of activation were evaluated along the path by using the quantum mechanical harmonic oscillator approximation in $3N_1 - 1$ degrees of freedom; the reaction coordinate was removed from this part of the calculation by a rank-1 projection operator.[21] The Hessians required for this step are computed by finite differences, and this is the expensive part of the calculation. The maximum of the generalized free energy of activation was found by Lagrangian interpolation; this maximum was used to calculate the rate constant by canonical variational theory[4-6] (CVT), which is VTST for a canonical ensemble.[30] The VTST rate constant is the one-way equilibrium flux from reactants to products through the variational transition state.[4-6] VTST includes classical recrossing effects at the conventional transition state to the extent that the trajectories that recross the conventional transition state do not recross the variational transition state.[4] Therefore the VTST rate constant is smaller than (or equal to) the rate constant predicted by conventional transitional state theory. The VTST calculations are semiclassical in that they treat vibrations quantum mechanically, but motions in the reaction coordinate are still classical. This classical aspect is corrected by including a transmission coefficient.

The transmission coefficient for the proton-transfer reaction was calculated using the microcanonical optimized multidimensional tunneling approximation,[31] which is based on a semiclassical approximation of the imaginary part of the analytically continued imaginary action integral along multidimensional tunneling paths from reactants to products.[31-33] The transmission coefficient also includes nonclassical reflection by the barrier.[34] We found that small-curvature[32,33] tunneling paths are more important than large-curvature[31,33] ones. Hence tunneling and nonclassical reflection along the reaction path were added by the small-curvature tunneling[32] (SCT) approximation.

The CVT and CVT/SCT rate constants can be used to calculate improved free energies of activation by eq 1. Such phenomenological activation parameters include dynamical (nonsubstantial) effects implicitly.[35]

Finally the reaction path, CVT, and CVT/SCT calculations were repeated for isotopically substituted reactions.

All calculations are at $T = 300$ K.

4. Results and Discussion

The rate constants and free energies of activation at three semiclassical levels of theory are given in Table 1. For comparison we also give the results of purely classical calculations in which all vibrations are treated by classical mechanics, and tunneling and nonclassical reflection are neglected. Table 1 shows that quantum effects are large, increasing the rate

Table 1. Rate Constants and Free Energies of Activation for the Conversion of 2-PGA to PEP by Enolase at 300 K

		k (s^{-1})	ΔG_{300}^{act} (kcal/mol)
semiclassical[a]	TST[b]	169	14.5
	CVT[c]	129	14.7
	CVT/SCT[d]	214	14.4
classical[a]	TST[b]	3.91	16.7
	CVT[c]	3.83	16.8
experiment		78	15.0

[a] "Semiclassical" denotes quantum mechanical vibrational partition functions; "classical" denotes classical mechanical vibrational partition functions. [b] "TST" denotes conventional transition state theory, i.e., the transition state is at the saddle point. [c] "CVT" is canonical-ensemble variational transition state theory in which the location of the transition state is chosen to maximize ΔG_T^{act} in the absence of tunneling. [d] "CVT/SCT" denotes CVT plus a small-curvature-tunneling transmission coefficient.

Table 2. Primary Kinetic Isotope Effect for Deuteron Transfer at 300 K

		k_H/k_D			k_H/k_D
semiclassical	TST	4.7	classical	TST	1.4
	CVT	3.7		CVT	1.3
	CVT/SCT	3.5	experiment		3.3

constant by a factor of 34 when quantum mechanical effects on the reaction coordinate are neglected and 56 when they are included. Classical free energies of activation differ from quantal ones by more than 2 kcal/mol.

The fact that the CVT/SCT rate constant differs from experiment more than the CVT rate constant does is probably an indication that the effective barrier in the present calculation, although realistic, is quantitatively a little low. The goal here is not to make quantitative evaluations of absolute rates but rather to gain insight into the importance of quantum mechanical nuclear motions in enzyme catalysis.

One way to test the theoretical method is to calculate the kinetic isotope effect (KIE) for deuteron transfer. The results are in Table 2. We find excellent agreement with experiment when quantum effects are included, but not when the calculations are classical. Furthermore, the results show that the correct KIE can be obtained only by going beyond conventional transition state theory. The reason for this is shown in Figure 2, which compares the CVT geometries for proton and deuteron transfer. For proton transfer, the CVT transition state has $r_1 = 1.75$ Å and $r_2 = 1.12$ Å, whereas for deuteron transfer the CVT transition state has $r_1 = 1.57$ Å and $r_2 = 1.26$ Å, with these latter values deviating less than 0.01 Å from their values at the saddle point. The variational transition state deviates from the saddle point for the H$^+$ transfer case primarily because the zero-point energy associated with the forming N−H bond increases more rapidly than the potential energy decreases just after one passes the saddle point. For D$^+$ transfer the zero-point energy of the N−D bond is smaller, and the vibrational contribution is not large enough to significantly alter the location of the dynamical bottleneck. As a consequence $k^{CVT}/k^{TST} = 0.76$ for H$^+$ transfer and 0.99 for D$^+$ transfer, which accounts for the smaller KIE at the CVT level. Adding quantum mechanical effects on reaction coordinate motion increases the H$^+$ transfer rate constants by a factor of 1.66, but this is more than canceled by an increase of 1.74 for D$^+$ transfer. Although one would

(29) Garrett, B. C.; Redmon, M. J.; Steckler, R.; Truhlar, D. G.; Baldridge, K. K.; Bartol, D.; Schmidt, M. W.; Gordon, M. S. *J. Phys. Chem.* **1988**, *92*, 1476−1488.

(30) Laidler, K. J. *Chemical Kinetics*, 3rd ed.; Harper & Row: New York, 1987.

(31) Liu, Y.-P.; Lu, D.-h.; González-Lafont, A.; Truhlar, D. G.; Garrett, B. C. *J. Am. Chem. Soc.* **1993**, *115*, 7806−7817.

(32) Liu, Y.-P.; Lynch, G. C.; Truong, T. N.; Lu, D.-h.; Truhlar, D. G.; Garrett, B. C. *J. Am. Chem. Soc.* **1993**, *115*, 2408−2415.

(33) Lu, D.-h.; Truong, T. N.; Melissas, V. S.; Lynch, G. C.; Liu, Y.-P.; Garrett, B. C.; Steckler, R.; Isaacson, A. D.; Rai, S. N.; Hancock, G.; Lauderdale, J. G.; Joseph, T.; Truhlar, D. G. *Comput. Phys. Commun.* **1992**, *71*, 235−262.

(34) Garrett, B. C.; Truhlar, D. G. *J. Phys. Chem.* **1979**, *83*, 2921−2926.

(35) Truhlar, D. G.; Garrett, B. C. *J. Am. Chem. Soc.* **1989**, *111*, 1232−1236.

(36) (a) Truong, T. N.; McCammon, J. A. *J. Am. Chem. Soc.* **1991**, *113*, 7504−7508. (b) Storer, J. W.; Houk, K. N. *J. Am. Chem. Soc.* **1993**, *115*, 10426−10427. (c) Corchado, J. C.; Espinosa-García, J. *J. Chem. Phys.* **1996**, *105*, 3160−3167. (d) Villà, J.; González-Lafont, A.; Lluch, J. M. *J. Phys. Chem.* **1996**, *100*, 19389−19397.

Table 3. Secondary Kinetic Isotope Effect for $-N_\epsilon D_2$ substitution at 300 K

semiclassical		k_H/k_D	classical		k_H/k_D
	TST	0.89		TST	1.00
	CVT	0.96		CVT	1.00
	CVT/SCT	0.96			

not find more D^+ tunneling than H^+ tunneling in one-dimensional theories of tunneling (in which the barrier height and shape do not depend on isotopic substitutions), the opposite situation is not unusual for multidimensional tunneling when the tunneling effect is small.[36] The origin of the effect is that the effective barrier for tunneling includes zero-point energy contributions for motions transverse to the tunneling path.[37] Proton tunneling can release more zero-point energy into the reaction coordinate, resulting in a lower, wider barrier than for deuteron transfer. Lower, wider barriers lead to smaller thermally averaged tunneling probabilities for a given energy decrement below the effective barrier top. Usually this effect is dominated by the change in effective reduced mass along the tunneling path due to the change in the mass of the transferred particle; however, when the barrier shape effect is dominant,[36] proton-transfer transmission coefficients will be smaller than those for deuteron transfer.

A more challenging test of theory is the prediction of a KIE that has not been measured. For this purpose we considered the secondary deuterium kinetic isotope effect for substituting deuterium for the hydrogens at N_ϵ. The results are in Table 3. In this case we see that the deviation from unity is decreased by a factor of 3 by including variational effects. Furthermore, the quantum effects are also large. For the $N_\epsilon D_2$ case, the variational transition state is 0.231 Å past the saddle point, leading to $k^{TST}/k^{CVT} = 1.41$, whereas for the $N_\epsilon H_2$ case, it is only 0.225 Å past the saddle point, leading to $k^{TST}/k^{CVT} = 1.32$. Therefore the secondary KIE is 1.07 larger at the CVT dynamical level than the TST one. Several isotopically sensitive frequencies contribute to this effect.

To check the accuracy of the rule of the geometric mean[38] for this reaction, we estimated the value of the rate constant for the D^+ transfer after substituting deuterium for the protiums at N_ϵ. The KIE obtained at the CVT/SCT level of calculation is 3.1, while the rule of the geometric mean gives a KIE of 3.4 (obtained by multiplying the primary KIE times the secondary KIE). The 10% deviation of these numbers exceeds the 4% secondary KIE; hence the rule of the geometric mean is not appropriate for this reaction, due to neglect of the variational location of the dynamical bottleneck and the multidimensional character of the tunneling effects. It would be dangerous to assume that these effects are unimportant for some reactions just because the rule of geometric mean is found experimentally to be approximately (∼10%) satisfied.

The Mg^{2+} ions clearly play an essential role in the stabilization of the transition state where the formal charge of the carboxylate group of the substrate changes from -1 to -2 as an enolate. Increased electrostatic interactions with both Mg^{2+} largely offset the energy cost of proton abstraction, which would be very unfavorable in the gas phase. Charge transfer and charge polarization of Mg^{2+} are missing in the present calculation, but charge polarization of the substrate is present. To test if the treatment of Mg^{2+} is reasonable, we carried out gas-phase Hartree−Fock calculations with the 6-311+G(d,p) basis set;

these calculations include charge transfer and full charge polarization, and they yield binding energies of -369 and -603 kcal/mol for $CH_3-CO\cdots Mg^{2+}$ and $CH=CO\cdots Mg^{2+}$, respectively. The corresponding AM1-GHO-CHARMM22 energies are -361 and -609 kcal/mol. The $-CO_2^-$ structure is nearly C_s, and the $=CO_2^{2-}$ structure is C_{2v}. The calculated energetics confirm that an MM treatment of Mg^{2+} is reasonable for this system since the transition state stabilization is primarily electrostatic. In addition to electrostatic stabilization by Mg^{2+}, there is electrostatic interaction between the increased positive charge on Lys 345 and the neighboring Asp 320 carboxylate residue (which is also coordinated to the metal ion). On the basis of the calculation in Section 2, we estimate a total stabilization energy to achieve a nearly thermoneutral reaction in the enzyme is about 290 kcal/mol, of which about $200-250$ kcal/mol may be gained by increased interaction energy from $CH_3-CO_2^-\cdots Mg^{2+} \rightarrow CH=CO_2^{2-}\cdots Mg^{2+}$.

The most obvious area for further developing the method is systematizing the choice of a configuration for the protein−water framework. In general the coordinates of the secondary-zone atoms can be assigned in a variety of ways. For example, they may be obtained from an X-ray structure or from the average geometry of a constrained molecular dynamics simulation. In the present work we carried out a constrained classical simulation, and we selected a representative geometry such that the relative energies of stationary points obtained in the second step have reasonable values. The model is not constrained as to the finer details such as contributions of various possible light-atom and heavy-atom motions to the reaction coordinate, the curvature of the reaction path, or the width of the effective barrier along the tunneling path. These reaction attributes are consequences of the AM1-GHO-CHARMM22 potential function, and it is very encouraging that this potential leads to such good agreement with experiment, even with the Mg^{2+} atoms treated by MM. It will be interesting to explore more systematic approaches in further work, including CVT calculations based on an ensemble of structures, and also to explore convergence as N_1 increases.

It is interesting to comment on other approaches to including quantum effects on enzyme reactions. The chief alternative to the SC-VTST method employed here for including quantum mechanical effects in rate constant calculations for multidimensional systems is path-integral quantum-mechanical transition state theory[39−41] (PI-QTST). This theory has been applied to enzyme reactions by Hwang and Warshel.[40,41] For carbonic anhydrase they found that quantum mechanical effects are small but nonnegligible.[41] The PI-QTST approach has been reviewed and compared to the SC-VTST approach (which is also called VTST with multidimensional tunneling or VTST/MT) in a previous paper;[42] in cases where PI-QTST and SC-VTST methods have been applied to the same problem, they give similar results.[43,44]

The present treatment is based on 75 degrees of freedom of the substrate and the catalytic base moving in the static electrostatic and van der Waals fields of the rest of the enzyme.

(37) Truhlar, D. G.; Kuppermann, A. *J. Am. Chem. Soc.* **1971**, *93*, 1840−1851.

(38) Bigeleisen, J. *J. Chem. Phys.* **1955**, *23*, 2264−2267.

(39) (a) Gillan, M. J. *J. Phys. C* **1987**, *20*, 3621−3641. (b) Voth, G. A.; Chandler, D.; Miller, W. H. *J. Chem. Phys.* **1989**, *91*, 7749−7760.

(40) Hwang, J.-K.; Chu, Z. T.; Yadav, A.; Warshel, A. *J. Phys. Chem.* **1991**, *95*, 8445−8448.

(41) Hwang, J.-K.; Warshel, A. *J. Am. Chem. Soc.* **1996**, *118*, 11745−11751.

(42) Truhlar, D. G.; Garrett, B. C.; Klippenstein, S. J. *J. Phys. Chem.* **1996**, *100*, 12771−12800.

(43) McRae, R. P.; Schenter, G. K.; Garrett, B. C.; Haynes, G. R.; Voth, G. A.; Schatz, G. C. *J. Chem. Phys.* **1992**, *97*, 7392−7404.

(44) Wonchoba, S. E.; Truhlar, D. G. *J. Chem. Phys.* **1993**, *99*, 9637−9651.

In contrast, the model of Borgis and Hynes[45] includes one degree of freedom representing the substrate and base and another collective coordinate representing electric polarization of the solvent. The tunneling model used by Saunders[46] for kinetic isotope effects of organic reactions involving proton transfer is further reduced to only the former single coordinate, which is known to be qualitatively inaccurate.[5,6,47]

An advantage of SC-VTST over more fully quantum mechanical approaches is that the semiclassical method allows one to attribute the quantum mechanical effects to specific features of the potential energy surface. In the present case the dominant quantum mechanical effect on both $k(T)$ and the primary KIE is associated with the release of C(2)−H zero-point energy and eventually the increase of N−H zero-point energy as the reaction proceeds. A second quantum effect is tunneling, which is also significant.

5. Summary and Concluding Remarks

The application of semiclassical or quantum mechanical methods to enzyme reactions presents a great challenge due to the high dimensionality and complexity of the potential surfaces for such systems. The key element in the present dynamical treatment is use of the embedded cluster[21,44] model. The substrate and a portion of the protein are treated as a cluster embedded in a rigid protein−water framework. Even with the assumption of frozen framework during the proton transfer, the choice of the position of the framework particles is still problematic, but we chose a typical configuration that gives a reasonable barrier height and reasonable overall thermodynamics. With this choice we were able to include quantized vibrations and tunneling in the dynamics of the substrate and part of the protein. The rate constants and primary kinetic isotope effects are in good agreement with experiment, and we have predicted a secondary kinetic isotope effect.

Furthermore, we have shown that the results of a purely classical simulation are inaccurate, a result we have found earlier for nonbiological catalysis.[48] One should therefore view with caution the absolute values of rate constants and free energies of activation calculated by the popular classical[2,3,49] simulation techniques, especially when there is significant hydrogenic motion in the reaction coordinate.

(45) Borgis, D.; Hynes, J. T. In *The Enzyme Catalysis Process: Energetics, Mechanism, and Dynamics*; Cooper, A., Houben, J. L., Chieu, L. C., Eds.; Plenum: New York, 1989; pp 293−303.

(46) (a) Saunders: W. H., Jr. *Techniques Chem. (N.Y.)*; 4th ed., **1985**, *6*/Part 1, 565−611. (b) Saunders, W. H., Jr. *J. Am. Chem. Soc.* **1985**, *107*, 164−169.

(47) (a) Garrett, B. C.; Truhlar, D. G. *Proc. Natl. Acad. Sci. U.S.A.* **1979,** *76*, 4755−4759. (b) Garrett, B. C.; Truhlar, D. G. *J. Chem. Phys.* **1980**, *72*, 3460−3471. (c) Skodje, R. T.; Truhlar, D. G. *J. Chem. Phys.* **1982**, *77*, 5955−5976. (d) Lu, D.-h.; Maurice, D.; Truhlar, D. G. *J. Am. Chem. Soc.* **1990**, *112*, 6206−6214. (e) Truhlar, D. G.; Lu, D.-h.; Tucker, S. C.; Zhao, X. G.; Gonzalez-Lafont, A.; Truong, T. N.; Maurice, D.; Liu, Y.-P.; Lynch, G. C. *ACS Symp. Ser.* **1992**, *502*, 16−36.

(48) Espinosa-García, J.; Corchado, J. C.; Truhlar, D. G. *J. Am. Chem. Soc.* **1997**, *119*, 9891−9896.

(49) Jorgensen, W. L. *Acc. Chem. Res.* **1989**, *22*, 184−189.